International Journal of Marine Energy 14 (2016) 215–228

Contents lists available at ScienceDirect

International Journal of Marine Energy

journal homepage: www.elsevier.com/locate/ijome

Physical testing of performance characteristics of a novel drag-driven vertical axis tidal stream turbine; with comparisons to a conventional Savonius

Tom Harries *, Alan Kwan, James Brammer, Roger Falconer

Hydro-environmental Research Centre, School of Engineering, Cardiff University, The Parade, Cardiff, UK

ARTICLE INFO

Article history:
Received 8 October 2014
Revised 12 January 2016
Accepted 27 January 2016
Available online 2 February 2016

Keywords:
Vertical-axis turbine
Savonius turbine
Tidal stream
IFREMER
Blockage effects

ABSTRACT

An experimental study of the performance and optimisation of a prototype novel drag-driven vertical axis tidal stream turbine is presented. The drag turbine has several unique advantages, including simple blade design, deployable in shallow waters and potential denser array spacing. Performance optimisation was conducted in the hydraulics flume at Cardiff University (CU), where the turbine reached $C_p\text{max}/\lambda = 0.132/0.441$ for its 90° phase angle configuration. The CU turbine was then tested using the wider and deeper hydraulics flume at IFREMER, France. Testing at IFREMER reduced the blockage factor from 17% at CU down to 1%; into the range of unblocked conditions. Testing in an unblocked environment, under similar flow conditions, reduced the peak efficiency of the CU turbine by 43% to $C_p\text{max}/\lambda = 0.067/0.346$. Finally the CU turbine was compared to the performance of a Savonius turbine. The design of the Savonius was based on a literature review. The CU turbine showed inferior efficiency values compared to the performance of the Savonius. The Savonius reached $C_p\text{max}/\lambda = 0.098/0.962$ in unblocked conditions, 46% greater than $C_p\text{max}$ of the drag turbine.

* Corresponding author. Tel.: +44 7756518784.
E-mail address: tom.harries@live.com (T. Harries).

http://dx.doi.org/10.1016/j.ijome.2016.01.008
2214-1669/

1. Introduction

There is currently a growing global energy crisis that is driven predominantly by to two factors: climate change and energy security. The solution to the aforementioned problems is to reduce both the demand for energy and emissions. Reducing emissions can be achieved through becoming more energy efficient, alongside harnessing indigenous sources of renewable energy.

Of the variety of renewable energy sources available to the UK, including wind, biomass and solar, the least developed is marine energy. Marine energy sources include wave energy, tidal range and tidal stream energy. Wave energy suffers from the intermittency of wind energy, and a proposal to install a tidal barrage in the UK was rejected partially on the basis of environmental concerns [1]. Tidal stream energy is predictable and regarded as a more environmentally friendly alternative to a tidal barrage, but at a lower power density [2]. In 2011 the UK generated 1 GWh from marine energy sources, equating to 0.003% of the total electricity generated from renewable sources [3]. This is a very small amount compared to the Carbon Trust's 2004 estimate that the UK has around 50% of Europe's tidal energy resource, at around 17 TWh/yr, equating to 4% of the UK's energy supply; a conservative estimate compared to the Carbon Trust's updated 2011 report that up to 29 TWh/yr could be harnessed [4].

Although the first full scale tidal stream turbine was deployed over a decade ago in 2003 off the coast of Lynmouth, Devon, by Marine Current Turbines Ltd. [5], there is currently no market leader in the tidal stream energy sector. No developer has progressed past deployment of a single full scale device. However progress and development is on the horizon since the UK Crown Estate released leases for 41 wave and tidal sites for array deployment around the UK in 2013 [6]. The largest of these is the MeyGen project (partially owned by Atlantis Resources Corporation), with consent for a 398 MW tidal stream array [7]. The market is currently dominated by horizontal-axis tidal turbines (HATTs) targeting tidal streams in depths greater than 30 m. However, due to their flexible rotor geometry, vertical-axis tidal turbines (VATTs) are more suitable than HATTs for harnessing flows in shallow waters (<30 m). VATTs are able to maintain their swept area in shallow depths through extending laterally. The shallow water resource is estimated at 1.1 TWh/yr around the UK, equating to 5% of the total UK tidal stream resource [8]: A significant untapped resource. A further advantage of VATTs is omni-directionality. Unlike HATTs, VATTs do not require a yawing system. Minimising design complexity is a key driver to reducing maintenance requirements and ensuring high reliability and availability of tidal stream turbines. In addition, omni-directionality reduces the risk of yaw misalignment, which can induce fatigue issues and be detrimental to performance [9].

This research describes the design of a power take-off system (PTO) to test and optimise the concept of a novel drag force harnessing VATT, herein referred to as the turbine, a conventional Savonius rotor [10] and their subsequent power characteristics. Despite typically reaching lower efficiencies than lift driven HATTs and VATTs, the simple blade designs of drag driven turbines, compared to the precise engineering of a hydrofoil, means that such turbines are appealing to less developed populations and in remote locations.

The objective of design optimisation of the turbine was to obtain power characteristics for a range of phase angles. The study was carried out in a re-circulating hydraulics flume at both Cardiff University's School of Engineering (CU) and at IFREMER, Boulogne-Sur-Mer, France. A Savonius rotor was tested, since the Savonius is largely regarded as the industry's leading drag-type turbine and is therefore used as the benchmark for the performance of the novel turbine. Despite the Savonius being regarded as a drag driven rotor, studies have shown the added presence of lift force [11–13].

2. The turbine

Conceived at CU and shown in Fig. 1, the CU turbine consists of a series of flat rectangular blades that are either closed or open. When closed in zone "*A*", the flaps act as bluff bodies generating form drag in the direction of the flow (positive torque). When open in zone "*C*" the flaps are parallel to the flow and act as streamlined bodies generating minimal frictional drag force (negative torque). The net

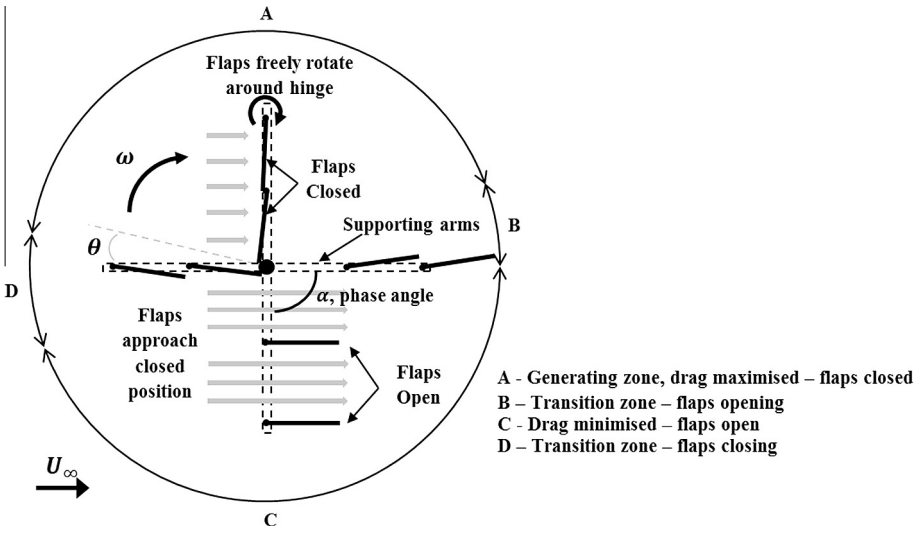

Fig. 1. The turbine working principles (plan view) for $\alpha = 90°$.

result is a rotary motion in the positive direction. Fig. 1 describes the CU turbine with a phase angle, $\alpha = 90°$, i.e. it has 4 "arms" with flaps attached. Contrary to the market dominant HATTs, the CU turbine harnesses a drag force as opposed to the conventionally harnessed lift force and is therefore a high torque and low angular velocity turbine. Potential unique advantages of the CU turbine include: simple blade design, deployable in shallow waters and potential denser array spacing. This is achieved, for example, through aligning two turbines along the axis of the streamwise direction of the flow. Generating power from only one half of the turbine potentially enables overlapping turbines. A denser array spacing can lead to an increased value of W/m^2, less ancillary equipment (e.g. inter-array cables) and easier array maintenance.

2.1. Numerical prediction of performance

Manwell et al. [14] calculated the theoretical $C_p - \lambda$ curve of a drag driven vertical axis wind turbine comprising flat plates, whereby the returning blades are shielded from the flow. The peak performance of the rotor was estimated at $C_p\text{max}/\lambda = 0.08/0.40$. Despite the $C_p$max being lower than the estimated cut off point of 0.30 for a perceived economically feasible tidal turbine [15], Manwell et al. [14] only analysed a 2-arm configuration $\alpha = 180°$ of a single flat plate for a static case. This study quantifies the dynamic performance of a drag-driven turbine with $\alpha < 180°$ with flaps opening and closing; unlike the rigid geometry of the Manwell et al. analysis [14]. Additionally, the turbine design benefits from omni-directionality, slow rotation and simple blade design that could go some way to balance the predicted reduced $C_p$max compared to conventional and market leading HATTs.

2.2. Competing technologies

A technology review of drag driven VATTs highlighted three key competitors: FlipWing [16], TIDENG [17] and the Hunter turbine, although published literature is only available for the Hunter turbine [18,19]. The Hunter turbine utilises the principle of opening and closing flaps, similar to the tur-

bine in this study, but the flaps are curved and hinged on a central cylinder. Physical testing of the Hunter turbine resulted in a peak performance of $C_p\text{max}/\lambda = 0.15/0.67$ [19].

3. Approach

This section contains details of the test facilities, design of both models (i.e. the CU turbine and the Savonius) and the performance capturing techniques.

3.1. Description of test facilities

The tests were carried out using re-circulating hydraulics flumes at two different facilities: CU, seen in Fig. 2(a), and IFREMER, Boulogne-Sur-Mer, France, seen in Fig. 2(b). The properties of the test facilities are presented in Table 1. In both facilities the models were centred within the flume cross-section and positioned at a set distance away from the inlet at which steady flow was established. IFREMER has previously been used for testing tidal turbines [20–24].

3.2. Model descriptions

The experimental models were designed and manufactured at CU. Both the geometry of the CU turbine and the Savonius turbine were of equal swept area, i.e. $A = DH$. A rotor diameter, $D = 400$ mm and height, $H = 250$ mm were chosen as a balance between maximising the generated torque, T (to reduce the influence of losses from the PTO on the results) and ensuring that the blockage factor, γ was kept to a minimum. The geometry of both models was sandwiched between two 2 mm thick disks. This not only ensured consistency in the flaps and bucket support between the CU turbine and the Savonius turbine, but also facilitated changes to the phase angle, α of the turbine that leads to design optimi-

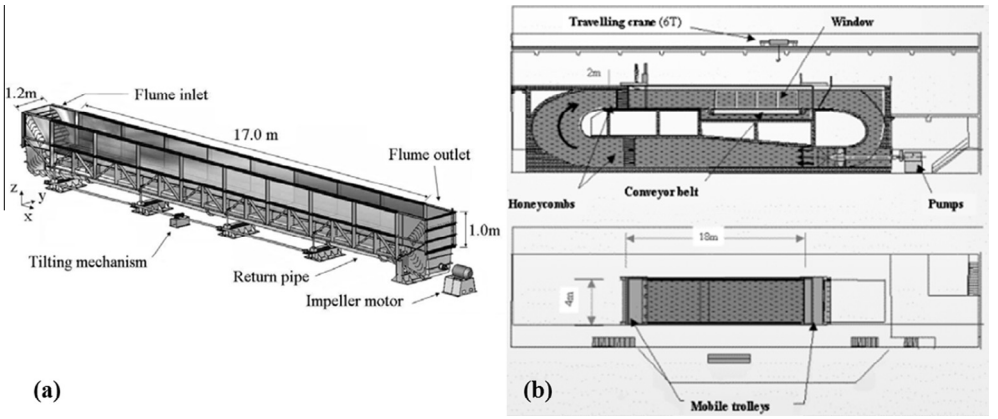

Fig. 2. Re-circulating hydraulics flumes at: (a) CU [25] and (b) IFREMER [20].

Table 1
Flume working section parameters for the CU and IFREMER [20,21] flumes.

Variable		Unit	CU	IFREMER
Length	X	m	17	18
Breadth	Y	m	1.2	4
Depth	Z	m	0.5	2
Max flow speed	U_∞	m/s	≈1.7	2.2

sation. Sandwiching the flaps between two disks enabled flap positions to be changed by drilling the positions of new holes in both disks, as opposed to manufacturing new supporting arms each time. The inclusion of disks/end plates has been shown to increase the performance of a Savonius rotor [26,27]. The turbines and all their fixings were manufactured from stainless steel.

The support structure used for the models at both CU and IFREMER can be seen in Fig. 3(b) and (c) respectively. Both structures had two stainless steel thrust bearings located in the base (submerged) and directly below the disk brake of the PTO (dry). To ensure consistency, the same bearings were used at both facilities.

3.2.1. CU turbine

The variable during testing of the CU turbine was the angle between adjacent arms, the phase angle, α, as shown in Fig. 4. For each configuration, each arm supported two flaps, except for T6. To avoid flap collisions, T6 consisted of three arms with two flaps and three arms with outer flaps only, as shown in Fig. 4. Two flaps per arm were chosen, since having a single flap per arm would restrict the

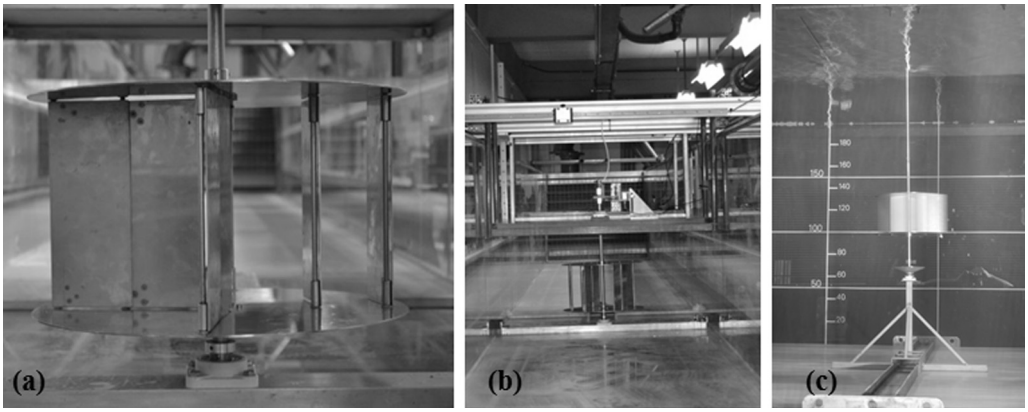

Fig. 3. Model images: (a) Side view of CU turbine $\alpha = 90°$, (b) support structure at CU and (c) support structure at IFREMER.

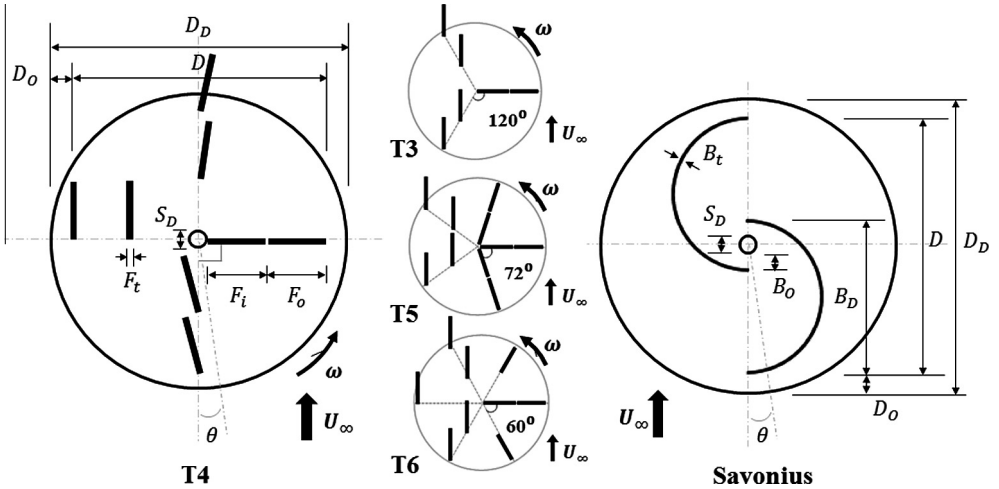

Fig. 4. CU Turbine (including various α) and Savonius schematics (plan view).

minimum phase angle, as flaps would collide for phase angles, $\alpha < 90°$. Each flap, cut from 2 mm stainless steel sheet, was hinged upon an axis extending the height of the turbine as shown in Fig. 3a. Each axis was tapped and screwed to the disk at each end. As shown in Fig. 3a, the rotation of the inner flap F_i was restricted by stoppers, positioned adjacent to the central shaft, whereas the rotation of the outer flap F_o was restricted by the axis of F_i. A clearance of 1 mm was maintained between both the top and bottom edge of each flap through the inclusion of washers.

3.2.2. Savonius

A review of the many permutations of the Savonius turbine resulted in an optimum configuration of a single stage [28,29], 2 bucket [30–32] with an overlap, B_0 [11]; as shown in Fig. 4, with dimensions listed in Table 2. Testing of a Savonius model was required due to the absence of a universal agreement or convergence on the efficiency of the Savonius. Design variables in the literature include helical blades, aspect ratio, bucket shape, stators and the variation in Reynolds number from wind and hydraulic testing.

3.3. Description of the power take-off (PTO)

A mechanical PTO, based on a disk brake, was designed and manufactured at CU, as shown in Fig. 5. Other studies using a mechanical PTO typically employed a dynamometer and a disk brake [33–35]. The load was applied to the rotor via a calliper, with friction being applied to the disk between two PTFE pads. The torque, T of the turbine was measured via a fixed $50N \pm 0.5\%$ range load cell on a 100 mm lever arm. The output signal of the load cell was then amplified through a signal-conditioning module and multiplied by the calibration factor. An in-line quadrature rotary shaft encoder positioned on top of the shaft, measured the angular velocity, ω with 2000 pulses per revolution; resulting in the rotated angle being measured every 0.18°. Both the encoder and load cell signals were streamed to a desktop PC through a USB connection, via a LabJack data logger. Results were collected at a frequency of 100 Hz for a sample period of 120 s. To visualise and record the data a bespoke data

Table 2
CU Turbine and Savonius dimensions (all in m).

Dimension	All	Dimension	CU turbine (T)	Savonius (S)
D	0.400	F_i	0.100	–
D_D	0.420	F_o	0.100	–
D_0	0.010	B_D	–	0.235
S_D	0.020	B_0	–	0.035
D_t, F_t	0.002	H	0.250	0.250

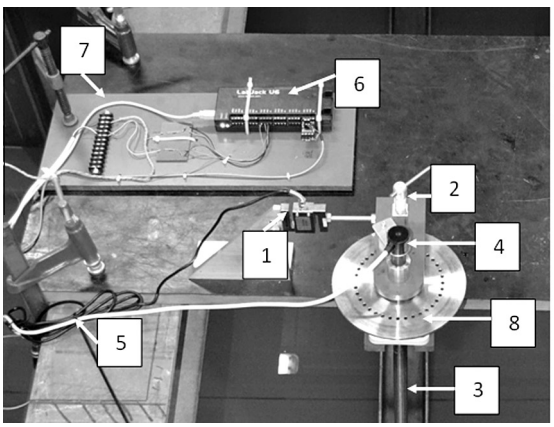

Component	Description
1	Load Cell
2	Load Applicator
3	Turbine Shaft
4	Encoder
5	Data cables to Labjack
6	Labjack
7	Data cable to PC
8	Brake Disk

Fig. 5. Annotated photograph of PTO components.

acquisition user interface was compiled using DaqFactory Express. This enabled the synchronisation of the encoder and load cell data, producing T and ω vs. θ data sets.

3.4. Description of flow characterisation

The flow conditions were measured using a Nortek ADV at CU, whilst the flow conditions at IFREMER were taken from Gaurier et al. [36]. Measuring the flow speed using the Nortek ADV resulted in 3D point measurements (i.e. streamwise U_x, spanwise U_y and depthwise U_z) of the flow speed within the test section. The freestream flow speed U_∞ was calculated as the resultant of the three flow speed components: U_x. U_y and U_z. The non-dimensional flow speed U^* was calculated from the freestream flow speed U_∞ and the model swept area averaged freestream flow speed $\overline{U}_\infty$ using $U^* = U_\infty/\overline{U}_\infty$. The Nortek ADV sampled at a rate of 200 Hz and a time independency study was carried out to determine the sampling period of 120 s for each data point; deemed a compromise of both accuracy and time expense. Vertical profiles were measured every 100 mm in the Y direction, consisting of eight data points in the Z direction (with the X-position corresponding to the model test location). All results obtained using the Vectrino ADV were analysed using the WinADV software [37]. The software was used for batch processing and for de-spiking and filtering anomalous data due to the low signal strength based on correlation > 70% with SNR > 10%.

3.5. Blockage factor

Following design optimisation, the chosen turbine design was tested in the flume at IFREMER. Such testing was required since the blockage factor, $\gamma = DH/XY$, present in the flume at CU was 17%. Previous studies using wind tunnels recommend $\gamma = 1 - 10\%$ for tunnel testing [38–40]. Whelan et al. [41] conducted both a numerical and physical model study of the blockage effect and found $C_p$max and the range of λ to be reduced by 50% for an unblocked case compared to $\gamma = 0.64$; highlighting the importance of unblocked testing. Failing to account for blockage (for $\gamma > 10\%$) would result in exaggerated performance values when compared to open, unblocked conditions. Testing at IFREMER reduced the blockage factor from 17% at CU to 1% at IFREMER, in-line with recommendations from the aforementioned studies. Other studies have estimated the effect of blockage on performance using correction factors from numerical models [42]. All testing at IFREMER was conducted at flow speeds similar to that used during testing at CU to ensure consistent model Reynolds numbers.

3.6. Test programme

Design optimisation of the turbine, driven by achieving the maximum C_p value, $C_p$max, was completed for the following phase angles: $\alpha = 120°$ (3 arm-T3), 90° (4 arm-T4), 72° (5 arm-T5) and 60° (6 arm-T6), as shown in Fig. 4. Testing at CU was conducted for the CU turbine configurations and the Savonius for a range of freestream flow speeds, U_∞, to check for model Reynolds number, Re_m independency; where $Re_m = \overline{U}_\infty D/\nu$. Subsequent testing at IFREMER enabled quantification of the blockage effect to be assessed on the performance data collected at CU for both the optimised CU turbine and the Savonius. A singular flow speed was tested at IFREMER.

Prior to initialising the flumes, the models were aligned to ensure $\theta = 0°$ corresponding to an arm of the turbine (or bucket of the Savonius) being aligned parallel and facing the direction of the flow, as shown in Fig. 4, along with the frictional load on the disk brake being set to zero. The flow speed was then increased to the desired amount and the model free-wheeling (λ_{max}). Friction was applied incrementally via the disk break calliper until stall conditions were achieved (λ_{min}). Next, the friction was removed incrementally until free-wheeling conditions were achieved (λ_{max}). A data point was recorded at each increment. This programme was adopted to test for any hysteresis in the system.

3.7. Data reduction

The performance of tidal stream turbines is characterised using the coefficient of performance C_p. The non-dimensional parameter C_p is the ratio of the generated mechanical power, $\overline{P}$ to the maximum available power in the freestream flow, $\overline{P}_\infty$ through the swept area, $A = DH$. The generated power, $\overline{P} = \overline{T}\bar{\omega}$, was calculated from the time averaged torque, $\overline{T}$ and angular velocity $\bar{\omega}$ over a 120 s sampling period. The rotational speed of tidal stream turbines is captured via the non-dimensional parameter, tip speed ratio λ, where λ is the ratio of the of the tangential speed of the tip of the blade, $r\bar{\omega}$ to the freestream flow speed, $\overline{U}_\infty$. Thus the terms are defined as:

$$\text{Coefficient of Power,} \quad C_P = \frac{\overline{P}}{\overline{P}_\infty} = \frac{\overline{T}\bar{\omega}}{\frac{1}{2}\rho A \overline{U}_\infty^3} \tag{1}$$

$$\text{Tip speed ratio,} \quad \lambda = \frac{r\bar{\omega}}{\overline{U}_\infty} \tag{2}$$

C_p takes into account the losses due to the Lanchaster–Betz law and the internal mechanisms of a turbine. Originally accredited to the work of Betz [43], but later amended to include the work of Lanchester [44], thanks to Bergey [45], the Lanchaster–Betz limit stipulates that for a turbine with a small cross section in comparison to the operating domain, i.e. unblocked conditions, the maximum achievable C_p is 16/27 or 59%. Numerical studies of the efficiency of a turbine in a tidal channel were carried out in detail by Garrett and Cummins [46], who state that the Lanchaster–Betz limit is achieved when the "flow speed decreases to $2/3\overline{U}_\infty$ through the turbine and further to $1/3\overline{U}_\infty$ as the flow expands in the turbine wake"; the theory of which is based upon the power extraction from wind by an actuator disk. In scenarios whereby the turbine cross section is large in comparison to the domain dimensions, i.e. bounded flow, blockage effects become apparent which increase the maximum achievable C_p.

A combined uncertainty approach was used to provide the bias limits for C_p and λ [47–49]. The approach assumes a root mean square propagation of errors in the multiplied data reduction equations of C_p and λ. For a typical case, overall uncertainty (for 95% confidence) for C_p and λ was calculated as 2.0% and 0.5% respectively.

4. Results and discussion

4.1. Flow characterisation of test facilities

For testing at CU, four different flow conditions were characterised resulting in $\overline{U}_\infty = 0.77, 0.93, 1.07$ & 1.22 m/s with $Re_m = 3.07, 3.71, 4.22$ & 4.86×10^5 respectively. Testing at IFREMER was conducted for $\overline{U}_\infty = 0.77$ m/s and with $Re_m = 2.99 \times 10^5$.

From Fig. 6 the width and depth averaged flow speeds (for each flow condition) show little variation across both the height, H and diameter, D of the models and can be considered almost uniform in both the Z and Y directions at the location of the models at CU and IFREMER. Only a width averaged vertical profile was available for IFREMER. Fig. 6 highlights that the model swept area is free from any bed and wall shear effects, whilst being positioned below the increase flow speed present adjacent to the free surface.

4.2. CU testing

The results for the power coefficient, C_p vs. tip speed ratio, λ for the turbine configurations, T3, T4, T5 and T6 for various $\overline{U}_\infty$ are shown in Fig. 7 and summarised in Table 3. Each configuration for all values of $\overline{U}_\infty$ follow an inverted-U-shape with apexes, $C_p$max around $\lambda \approx 0.4$. The results show that the performance of T3, T4 and T6 follow similar distributions with $C_p\text{max} \approx 0.12$, whereas the performance of T5 is lower, with $C_p\text{max} \approx 0.09$. All the turbine configurations have a range of $0.1 \leqslant \lambda \leqslant 0.75$.

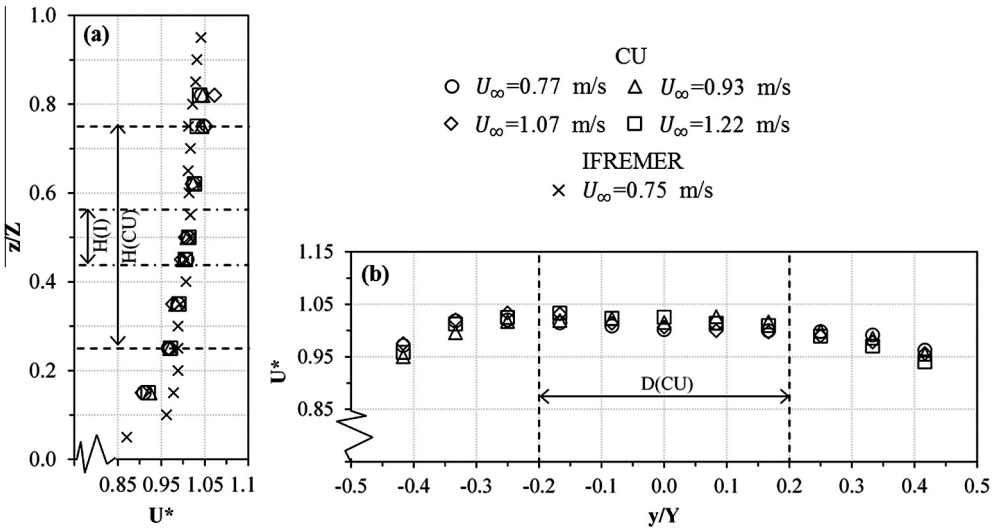

Fig. 6. ADV profiles for all flow conditions (a) width averaged U^* profiles at model location for CU and IFREMER (b) depth averaged U^* profiles at model location for CU.

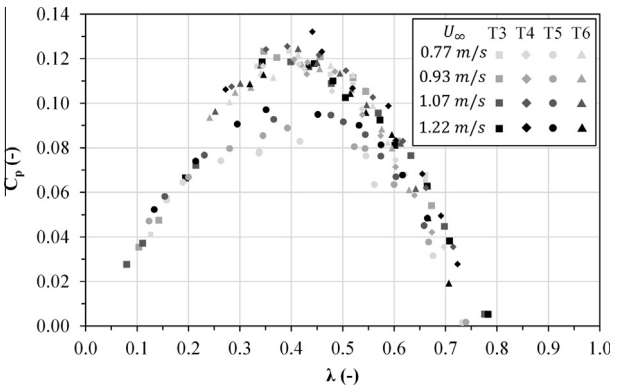

Fig. 7. C_p vs. λ for the turbine configurations at CU for various $\overline{U}_\infty$.

Table 3
$C_p$max/λ values for all models tested at CU.

$C_p$max/λ		T3	T4	T5	T6	Savonius
$\overline{U}_\infty$ (m/s)	Re_m($\times 10^5$)					
0.77	3.07	0.123/0.395	0.117/0.415	0.083/0.417	0.122/0.413	0.225/0.999
0.93	3.71	0.123/0.347	0.120/0.406	0.089/0.393	0.118/0.421	0.239/0.834
1.07	4.22	0.119/0.399	0.126/0.393	0.095/0.478	0.125/0.413	0.261/0.831
1.22	4.86	0.118/0.343	0.132/0.441	0.097/0.351	0.117/0.433	0.266/1.051

The reduction in C_p from T4 to T5 could be as a result of excess shadowing from numerous arms being present in the generating zone (i.e. zone *A* in Fig. 1) at any one point, hence reducing the unobstructed frontal area of the inner generating flaps and in turn reducing the generated torque and overall power.

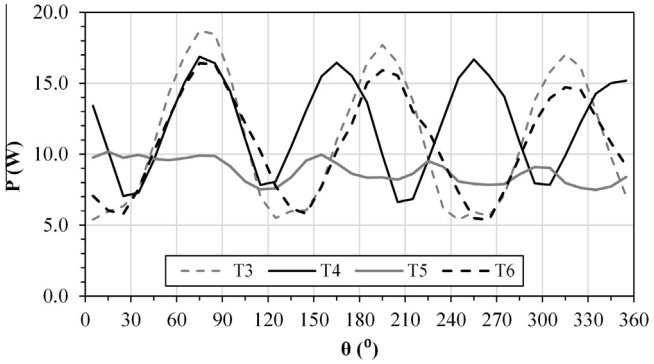

Fig. 8. P vs. θ for various α for $U_\infty = 1.22$ m/s at CU.

Table 4
Power characteristics over 360° for various α for $U_\infty = 1.22$ m/s for models tested at CU.

	T3	T4	T5	T6	Savonius
$\overline{P}(W)$	10.738	11.968	8.789	10.611	24.138
$\sigma(W)$	4.596	3.294	0.856	3.540	2.427
$\overline{T}$(Nm)	5.125	4.447	4.101	4.018	3.765
$\bar{\omega}$(rad/s)	2.095	2.692	2.143	2.641	6.411

In Fig. 7 and Table 3 it is noted that there is minimal difference in $C_p$max for each configuration for the various values of $\overline{U}_\infty$, with only T4 and T5 showing an increase in performance with increasing $\overline{U}_\infty$. Therefore the performance of the CU turbine could be deemed independent of the model Reynold's Number. Design optimisation resulted in the T4 configuration, i.e. α = 90°, achieving the highest performance, with for $C_p\text{max}/\lambda = 0.132/0.441$ for $\overline{U}_\infty = 1.22$ m/s.

The variation in power output over 360° for a range of α for $\overline{U}_\infty = 1.22$ m/s can be seen in Fig. 8. In addition the average power over 360° for a range of α are summarised in Table 4. As expected each configuration has a repeating pattern, based upon its phase angle, i.e. T4 has a period of 90°. The periodic behaviour reflecting the phase angle is also seen in the results of the Hunter Turbine [19]. For the first phase of each configuration P_{max} occurs at $65° \leqslant \theta \leqslant 75°$. The highest power output, 11.968 W was generated by T4, whilst T5 generated the lowest at 8.789 W. Besides the average power over 360°, the variation in power throughout the tidal cycle is also an important factor in power generation. Ideally the power output would be smooth with minimal fluctuations to reduce the degree of power conditioning required. The power fluctuation for various α in Fig. 8 is quantified using the standard deviation, σ and shown in Table 4. As the phase angle decreases from 120° (T3) to 72° (T5) the power fluctuation over 360° also decreases, as seen in σ reducing from 4.596 W to 0.856 W respectively. Unfortunately a decrease in σ with decreasing α also coincides with a decrease in $\overline{P}$ over 360°.

A comparison of the performance results, C_p vs. λ, of the Savonius against the highest performing CU turbine configuration, T4 for various $\overline{U}_\infty$, can be seen in Fig. 9 (with the performance summary being given in Table 3). Firstly the Savonius displays the expected inverted-U-shape with apex around $\lambda \approx 1.0$ and operates for $0.7 \leqslant \lambda \leqslant 1.7$, near double that of T4. Unlike the CU turbine, the performance of the Savonius is not independent of $\overline{U}_\infty$, with the performance increasing by nearly 20% from $\overline{U}_\infty = 0.77$ to 1.22 m/s. This is in-line with the analysis by Mason-Jones et al. [50], which states that for $Re_m < 10^6$ the performance is likely to be a function of $\overline{U}_\infty$. The peak performance of the Savonius, i.e. $C_p\text{max}/\lambda = 0.266/1.051$, was achieved at $\overline{U}_\infty = 1.22$ m/s and is 100% greater than the $C_p$max value

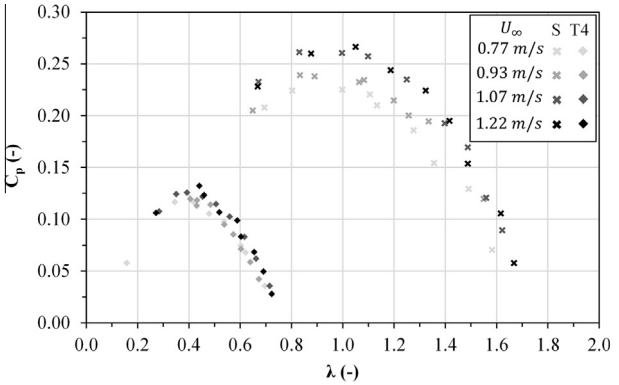

Fig. 9. C_p vs. λ for T4 and the Savonius at CU for various $\overline{U}_\infty$.

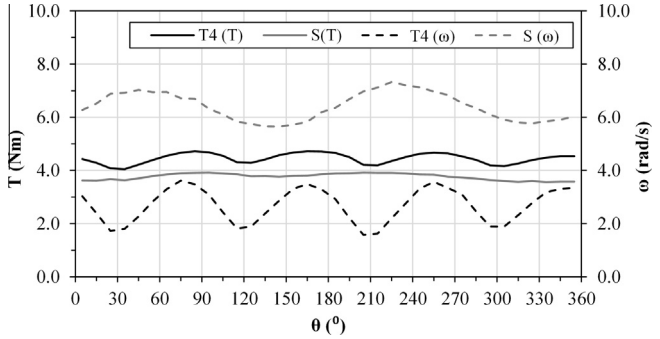

Fig. 10. Comparison of T, ω vs. θ for $C_p$max at $\overline{U}_\infty = 1.22$ m/s for T4 and the Savonius from Fig. 9.

for T4. In conjunction with Fig. 9, Fig. 10 deconstructs the power output of both T4 and the Savonius through displaying the varying torque, T and angular velocity, ω components ($P = T\omega$) over 360° at $C_p max$ for $\overline{U}_\infty = 1.22$ m/s (with the time averaged values being given in Table 4). It can be seen from Fig. 10 that both T and ω for both T4 and the Savonius turbines display a repeating pattern based upon their respective phase angles of 90° and 180° (i.e. 2 buckets). The inferior $C_p$max reached by T4 compared to the Savonius can be attributed to its low angular velocity, since T4 generates 18% greater torque than the Savonius over 360°; yet the Savonius rotates at an angular velocity 138% higher than T4.

4.3. IFREMER testing

Testing at IFREMER was conducted for the highest performing turbine configuration, T4 and the Savonius for $\overline{U}_\infty = 0.75$ m/s – a comparable speed to the one used at CU ($\overline{U}_\infty = 0.77$ m/s). Since at IFREMER for $\overline{U}_\infty = 0.75$m/s the free surface behaviour remained steady, whereas at higher $\overline{U}_\infty$ surface waves became apparent, which created additional unwanted loading on the models.

The influence of blockage effects can be seen in Fig. 11, which shows that there is a decrease in the $C_p$max value for both T4 and Savonius when tested at IFREMER compared to the value achieved while testing at CU. The Savonius showed the largest decrease in $C_p$max, 75% compared to 43% for the T4. In addition there is also a reduction in the corresponding λ value for $C_p$max, as well as the configurations achieving lower $\lambda_{\max}$ values (i.e. freewheeling conditions). As a result the $C_p - \lambda$ curves for both the T4 and Savonius turbines have been shifted downwards and to the left. Such a reduction was also found

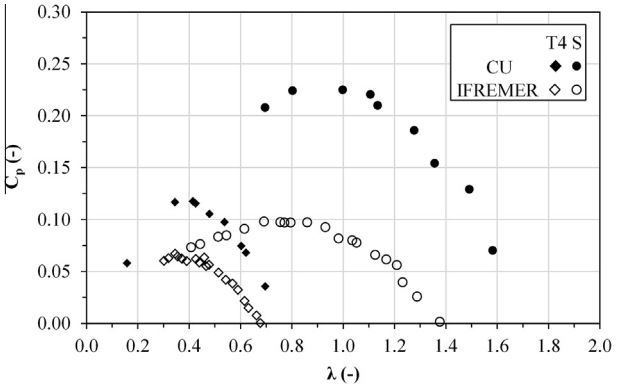

Fig. 11. C_p vs. λ for T4 and Savonius at CU and IFREMER for $\overline{U}_\infty = 0.75$ and 0.77 m/s respectively.

by Whelan et al. [41], who experienced a drop in $C_p$max of around 50% for an unblocked case compared to a highly blocked case.

The reason for T4 experiencing a lower reduction in $C_p$max at IFREMER compared to CU could be due to T4 allowing the freestream flow through half of its swept area, compared to the Savonius which provides a solid blockage for the entire swept area, resulting in a modified blockage factor of $\gamma = 8.3\%$ for T4, compared to $\gamma = 16.6\%$ for the Savonius. At CU this would result in a smaller acceleration of the freestream flow due to blockage when testing T4, since the model solidity and hence blockage is smaller. At $C_p$max the Savonius is rotating at more than double the rotational speed of T4, and as discussed by Chen and Liou [51] at higher values of λ a rotating turbine will act as more of a solid wall-inducing a greater degree of blockage to the flow, (until a limiting value of λ is reached) which could also explain why the Savonius experiences a larger decrease in performance at IFREMER compared to T4. Despite the downwards shift in the $C_p{-}\lambda$ curves, the CU and IFREMER data exhibit similar distributions for each of the models. However, the performance of the Savonius turbine remains superior to that of T4, with $C_p\text{max}/\lambda = 0.098/0.692$ for the Savonius compared to $C_p\text{max}/\lambda = 0.067/0.346$ for T4.

From Fig. 11 the low λ range ($\lambda \leqslant 1.0$) of the CU turbine was expected since the λ of a solely drag driven rotor is limited to $\lambda \leqslant 1.0$, as the tangential velocity of a drag driven rotor cannot exceed U_∞. Unlike T4, the Savonius can operate for $\lambda > 1.0$ since it generates a lift force and thus a greater angular velocity (as discussed in Section 4.2) [11–13]. The unblocked result for the T4 turbine, i.e. $C_p\text{max}/\lambda = 0.067/0.346$, is 16% lower than that predicted by Manwell et al. [14] ($C_p\text{max}/\lambda = 0.080/0.330$). Potentially the difference could be reduced through shielding the returning turbine flaps (i.e. zone *C* in Fig. 1), akin to Manwell's design. This would reduce the negative torque from the returning flaps due to skin friction drag, resulting in an overall net increase in torque and thus power. However, a shielding mechanism is not practical since this would eradicate one of the turbine's key advantages over HATT's: namely omni-directionality.

5. Conclusions

Models of both a novel drag-driven VATT (referred to herein as the CU turbine) and a conventional Savonius turbine were designed, manufactured and tested in two re-circulating hydraulics flumes. The power characteristics of the models, namely: power, torque and angular velocity, were measured using a bespoke mechanical disk brake power take-off system. Initial design optimisation of the novel CU turbine resulted in an optimum phase angle of 90°. An observation to note is that a decreasing phase angle leads to both a reduction in power fluctuation but also power output. To the authors' knowledge there was no literature on optimisation of a flat plate drag driven vertical-axis turbine design prior to this study. However, the performance of a conventional Savonius design proved supe-

rior to the novel CU turbine. It is hypothesised that the superior performance is primarily due to the additional lift force generated by the Savonius.

The results of model testing in the hydraulics flumes, with both a high and minimal blockage factor, highlight the importance of accounting for blockage effects during tank testing. Failure to account for the effects of blockage can lead to exaggerated performance results. Despite the low efficiency performance obtained for the CU turbine, this investigation is only an initial study and therefore further investigation into other design parameters, such as the aspect ratio, blade size and blade support could prove significant.

Acknowledgements

The work described in this paper has been funded by both a Knowledge Economy Skills Scholarship (KESS) in collaboration with TATA Steel and the Marine Renewables Infrastructure Network (MARINET). The authors would also like to acknowledge Paul Leach for his invaluable contributions.

References

[1] House of Commons, A Severn Barrage?: Government Response to the Committee's Second Report of Session 2013 and 2014, London, HC 622, 10 2013.
[2] D.J.C. MacKay, Sustainable Energy: Without the Hot Air, Uit Cambridge Limited, 2009.
[3] DECC, UK Energy in Brief 2012, National Statistics, 2012.
[4] Carbon Trust, Accelerating marine energy, DECC, London, July 2011.
[5] Marine Current Turbines, About Marine Current Turbines Marine Current Turbines, Available online: http://www.marineturbines.com/About-Marine-Current-Turbines (accessed: 06.10.2014).
[6] The Crown Estate, Leasing round and projects, 22.05.2013. Available online: http://www.thecrownestate.co.uk/energy-infrastructure/wave-and-tidal/pentland-firth-and-orkney-waters/leasing-round-and-projects/ (accessed: 23.09.2013).
[7] The Crown Estate – First UK tidal array project agrees funding. Available online: http://www.thecrownestate.co.uk/news-and-media/news/2014/first-uk-tidal-array-project-agrees-funding/ (accessed 06.10.2014).
[8] Black and Veatch Consulting Ltd, PHASE II UK Tidal Stream Energy Resource Assessment, Carbon Trust, London, 107799/D/2200/03, July 2005.
[9] F. Maganga, G. Germain, J. King, G. Pinon, E. Rivoalen, Experimental characterisation of flow effects on marine current turbine behaviour and on its wake properties, IET Renew. Power Gener. 4 (6) (2010) 498–509.
[10] S.J. Savonius, The S-rotor and its applications, Mech. Eng. 53 (1931) 333–338.
[11] J.V. Akwa, H.A. Vielmo, A.P. Petry, A review on the performance of Savonius wind turbines, Renewable Sustainable Energy Rev. 16 (5) (Jun. 2012) 3054–3064.
[12] N. Fujisawa, F. Gotoh, Experimental study on the aerodynamic performance of a Savonius rotor, J. Sol. Energy Eng. 116 (3) (Aug. 1994) 148–152.
[13] M. Nakajima, S. Iio, T. Ikeda, Performance of Savonius rotor for environmentally friendly hydraulic turbine, J. Fluid Sci. Technol. 3 (3) (2008) 420–429.
[14] J.F. Manwell, J.G. McGowan, A.L. Rogers, Aerodynamics of wind turbines, in: Wind Energy Explained, John Wiley & Sons, Ltd, 2009, pp. 91–155.
[15] University of Southampton, Tidal-current Energy Device Development and Evaluation Protocol, UK Government, URN 08/1317, 2008.
[16] Hydrovolts, New Clean Technology, 2012. Available online: http://hydrovolts.com/ (accessed 17.09.2013).
[17] TIDENG, The rotor, 2013. Available online: http://www.tideng.com/Tideng/Tideng.html. (accessed: 17.09.2013).
[18] Y. Li, S.M. Calisal, Three-dimensional effects and arm effects on modeling a vertical axis tidal current turbine, Renewable Energy 35 (10) (Oct. 2010) 2325–2334.
[19] B. Yang, C. Lawn, Fluid dynamic performance of a vertical axis turbine for tidal currents, Renewable Energy 36 (12) (Dec. 2011) 3355–3366.
[20] P. Davies, G. Germain, B. Gaurier, A. Boisseau, D. Perreux, Evaluation of the durability of composite tidal turbine blades, Philos. Trans. A Math. Phys. Eng. Sci. 371 (1985) (Feb. 2013) 20120187.
[21] G. Germain, Marine current energy converter tank testing practices, presented at the 2nd International Conference on Ocean Energy (ICOE 2008), 15–17th October 2008, Brest, France, 2008.
[22] G. Germain, A.S. Bahaj, P. Roberts, C. Huxley-Reynard, Facilities for marine current energy converter characterization, presented at the 7th European Wave and Tidal Energy Conference (EWTEC), Porto, Portugal, 2007.
[23] F. Maganga, G. Germain, J. King, G. Pinon, E. Rivoalen, Experimental study to determine flow characteristic effects on marine current turbine behaviour, presented at the EWTEC 2009, Uppsala, 2009.
[24] L. Myers and A.S. Bahaj, Near wake properties of horizontal axis marine current turbines, in: Proceedings of the 8th European Wave and Tidal Energy Conference, 2009, pp. 558–565.
[25] W.B. Rauen, B. Lin, R.A. Falconer, Transition from wavelets to ripples in a laboratory flume with a diverging channel, Int. J. Sediment Res. 23 (1) (Mar. 2008) 1–12.
[26] I. Ushiyama, H. Nagai, and M. Mino, The optimum design configurations of savonius wind turbines, in IECEC '82, in: Proceedings of the Seventeenth Intersociety Energy Conversion Engineering Conference, 1982, vol. 1, pp. 2096–2101.
[27] J.-L. Menet and N. Bourabaa, Increase in the Savonius rotors efficiency via a parametric investigation, in: Proceedings of the European Wind Energy Conference, London, UK, 2004.

[28] K. Golecha, T.I. Eldho, S.V. Prabhu, Influence of the deflector plate on the performance of modified Savonius water turbine, Appl. Energy 88 (9) (Sep. 2011) 3207–3217.
[29] M.N.I. Khan, M.T. Iqbal, M. Hinchey, Submerged water current turbines, Oceans 2008 (2008) 1–6.
[30] U.K. Saha, S. Thotla, D. Maity, Optimum design configuration of Savonius rotor through wind tunnel experiments, J. Wind Eng. Ind. Aerodyn. 96 (8–9) (Aug. 2008) 1359–1375.
[31] R.E. Sheldahl, L.V. Feltz, B.F. Blackwell, Wind tunnel performance data for two-and three-bucket Savonius rotors, J. Energy 2 (3) (1978) 160–164.
[32] Z. Zhao, Y. Zheng, X. Xu, W. Liu, G. Hu, Research on the improvement of the performance of savonius rotor based on numerical study, in: International Conference on Sustainable Power Generation and Supply, 2009. SUPERGEN '09, 2009, pp. 1–6.
[33] S. Armstrong, A. Fiedler, S. Tullis, Flow separation on a high Reynolds number, high solidity vertical axis wind turbine with straight and canted blades and canted blades with fences, Renewable Energy 41 (May 2012) 13–22.
[34] S.-H. Han, J.-S. Park, K.-S. Lee, W.-S. Park, J.-H. Yi, Evaluation of vertical axis turbine characteristics for tidal current power plant based on in situ experiment, Ocean Eng. 65 (Jun. 2013) 83–89.
[35] M. Shiono, K. Suzuki, and S. Kiho, Output characteristics of Darrieus water turbine with helical blades for tidal current generations, in: Proceedings of the Twelfth International Offshore and Polar Engineering Conference, Kitakyushu, Japan, 2002, pp. 859–864.
[36] B. Gaurier, P. Davies, A. Deuff, G. Germain, Flume tank characterization of marine current turbine blade behaviour under current and wave loading, Renewable Energy 59 (Nov. 2013) 1–12.
[37] T.L. Wahl, WinADV, U.S. Department of the Interior - Bureau of Reclamation, 2012. Available online: http://www.usbr.gov/pmts/hydraulics_lab/twahl/winadv/ (accessed: 27.11.2013).
[38] E.C. Maskell, A theory of the blockage effects on bluff bodies and stalled wings in a closed wind tunnel, DTIC Doc. (1963).
[39] R.C. Pankhurst, D.W. Holder, Wind-tunnel Technique: An Account of Experimental Methods in Low-And High-Speed Wind Tunnels, Pitman, 1952.
[40] A. Pope, J.J. Harper, Low-speed wind tunnel testing, John Wiley & Sons, New York, 1966.
[41] J.I. Whelan, J.M.R. Graham, J. Peiró, A free-surface and blockage correction for tidal turbines, J. Fluid Mech. 624 (2009) 281–291.
[42] A.S. Bahaj, A.F. Molland, J.R. Chaplin, W.M.J. Batten, Power and thrust measurements of marine current turbines under various hydrodynamic flow conditions in a cavitation tunnel and a towing tank, Renewable Energy 32 (3) (Mar. 2007) 407–426.
[43] A. Betz, Das Maximum der theoretisch möglichen Ausnutzung des Windes durch Windmotoren, Z. Für Gesamte Turbinenwesen 26 (1920) 307–309.
[44] F.W. Lanchester, A contribution to the theory of propulsion and the screw propeller, Trans. Ins. Tion Nav. Archit. 57 (1915) 98–116.
[45] K.H. Bergey, The Lanchester-Betz limit, J. Energy 3 (Dec. 1979) 382–384.
[46] C. Garrett, P. Cummins, The efficiency of a turbine in a tidal channel, J. Fluid Mech. 588 (2007) 243–251.
[47] EquiMar, Deliverable 3.4: Best practice for tank testing of small marine energy devices, Commission of the European Communities, December 2010.
[48] R.A. McAdam, G.T. Houlsby, M.L.G. Oldfield, Experimental measurements of the hydrodynamic performance and structural loading of the transverse horizontal axis water turbine: Part 1, Renewable Energy 59 (Nov. 2013) 105–114.
[49] E.E. Lust, L. Luznik, K.A. Flack, J.M. Walker, M.C. Van Benthem, The influence of surface gravity waves on marine current turbine performance, Int. J. Mar. Energy 3–4 (Dec. 2013) 27–40.
[50] A. Mason-Jones, D.M. O'Doherty, C.E. Morris, T. O'Doherty, C.B. Byrne, P.W. Prickett, R.I. Grosvenor, I. Owen, S. Tedds, R.J. Poole, Non-dimensional scaling of tidal stream turbines, Energy 44 (1) (Aug. 2012) 820–829.
[51] T.Y. Chen, L.R. Liou, Blockage corrections in wind tunnel tests of small horizontal-axis wind turbines, Exp. Therm. Fluid Sci. 35 (3) (Apr. 2011) 565–569.